Arch. Metall. Mater. **63** (2018), 3, 1153-1165

DOI: 10.24425/123788

Z. NIE*#, Y. LIN*, Q. TONG**

COMPUTATIONAL MODELING OF THE ELASTIC PROPERTY OF THREE-DIMENSIONAL OPEN CELL FOAMS

The work reports on the development of random three-dimensional Laguerre-Voronoi computational models for open cell foams. The proposed method can accurately generate foam models having randomly distributed parameter values. A three-dimensional model of ceramic foams having pre-selected cell volumes distribution with stochastic coordinates and orientations was created in the software package ANSYS^{TM}. Different groups of finite element models were then generated using the developed foam modeling procedure. The size sensitivity study shows that each of foam specimens at least contains 125 LV-cells. The developed foam models were used to simulate the macroscopic elastic properties of open cell foams under uni-axial and bi-axial loading and were compared with the existing open cell foam models in the literature. In the high porosity regime, it is found that the elastic properties predicted by random Laguerre-Voronoi foam models are almost the same as those predicted by the perfect Kelvin foam models. In the low porosity regime the results of the present work deviate significantly from those of other models in the literature. The results presented here are generally in better agreement with experimental data than other models. Thus, the Laguerre-Voronoi foam models generated in this work are quite close to real foam topology and yields more accurate results than other open cell foam models.

Keywords: open cell foams, Laguerre-Voronoi tessellation, finite element method, elastic property, macrostructure

1. Introduction

Engineered cellular solids (foams) are used in a wide range of industrial applications [1], for example, light-weight structural components, insulation, and filtration, etc. Sponge and bone, the natural counterparts of cellular solids, can optimize the performance in a particular setting because of the cellular structure. Both open cell and closed cell microstructures are available in commercial foams, depending on the manufacturing technology. The macroscopic properties of open cell foams are determined by the materials of the solid portion, and more importantly by the microstructures of the foams, e.g., geometrical aspects. Examining the relationship between the physical properties of open cell foams to their relative density and complex microstructure is necessary to understand how those properties can be optimized for a given application and to identify more applications of foams [2-6].

The easily measured mm or μm microstructure size aids developing models of the relationship between the macroscopic mechanical properties and the microstructures of foams. Gibson and Ashby [7], and Banhart [8] report on the models describing the micro-mechanics of open cell foams. Many studies have investigated the effect of local cell features, e.g., strut shape, on the macrostructure properties of periodic foam structures. Some models are generalizable to real materials. Other studies have focused on how the randomness and imperfections of non-periodic structures, and the interaction between cells inside such structures affect cells-scale properties.

Models reviewed for this investigation fall into two categories. The first category includes models in which the repetitive unit cell is used to construct idealized foam behavior models, such as 2D models: honeycomb/foam cells [7,9-14] and 3D models: cubic cells, tetrahedral cells, and Kelvin cells [7,15-20]. T. Wejrzanowski et al. [21] proposed a three-dimensional model for open cell foams using Laguerre-Voronoi tessellation. They compared the porosity and surface area with experimental data, but did not study the elastic properties of open cell foams. The main drawback of this kind of model is over-prediction of yield strength and bulk modulus since such models do not include the irregular microstructures of real foams. The second approach of micromechanics modeling, i.e., so-called "super-cell models", has been proposed to provide a better understanding of the morphological structure of real materials, which considers the randomness and imperfections of irregular cells. Voronoi models are the most popular among the super-cell models. Gibson and Ashby [2] reported 2D Voronoi models and concluded that the mechanical responses of 2D Voronoi models under uni-axial loads are almost the same as that of idealized 2D foam models.

* UNIVERSITY OF MISSOURI, COLUMBIA, DEPARTMENT OF MECHANICAL AND AEROSPACE ENGINEERING, MO 65211 US
** BEIJING JIAOTONG UNIVERSITY, SCHOOL OF ELECTRICAL ENGINEERING, BEIJING, BEIJING 100044 CHINA
# Corresponding author: znhc5@mail.missouri.edu

They also found that the strength and stiffness of 2D Voronoi models would decrease sharply when deleting some cell edges under uni-axial loads.

Chen et al. [11] presented the effect of different microstructural defects on the macroscopic responses to external loading via introducing imperfections into the morphology of foam models. They reported an elliptical yield surface under multi-axial loads for elastoplastic foams. Most of the finite element analyses of 3D Voronoi models in the literature have focused on only the elastic properties [11,18,22-27]. Zhu et al. [28] analyzed 3D foam models with low relative density ρ (e.g., $\rho = 0.01$), and found that the shear modulus and Young's modulus of highly irregular foams are greater, and the bulk modulus is less, than a perfect foam. The Poisson's ratio does not change with the cell regularity, but increases gradually with decreasing relative density. The models in [28] can be regarded as isotropic on average and the stress-strain curves are still similar to that of perfect foams with different values of regularity.

The effects of foam models' disparity, such as the variation of cell sizes, the irregularity of cell shapes, and the imperfections of cell struts, upon the mechanical properties have been considered in [22,29,30]. Li et al. [31] analyzed the effects of co-existing cell strut imperfections and cell shape irregularity on the mechanical properties of 2D foam structures using the finite element method. They concluded that the shear modulus and Young's modulus of imperfect foams vary as a power-law function of the relative density when changing in cell strut thickness and cell shapes. Li et al. [32] developed a micromechanical model for evaluating the effective elastic properties of 3D foams in three different loading modes using Kelvin cell. The results show that the effective elastic properties of the foam are determined by the elastic properties of solid materials, the size and shape of the strut cross-section, and the relative density. Ćwieka et al. created 3D models with Laguerre-Voronoi tessellations and investigated the effect of the cell size on the elastic behavior of metallic foams [33].

In other studies recently, the digitized images or tomographic images of the foams are used to reassemble the 3D structures of real foams to obtain the mechanical properties of open cell foams [34-37]. X-ray micro-tomography (μCT) and magnetic resonance imaging (MRI) are very powerful tools that can capture the architecture and microstructures of materials in a non-destructive and non-invasive way. This approach also is called 3D reconstruction technology, which reconstructs a 3D model using 2D image slices such as μCT and MRI stacks. However, 3D models obtained this way are unable to represent all investigated foam structures. Such models are unique for each individual foam sample. Moreover, this technology is not always feasible since the reconstruction process is high-cost, complicated and time-consuming.

In this work, an alternative three-dimensional random Laguerre-Voronoi foam model was developed to predict the elastic properties of open cell ceramic foams. First, a three-dimensional model of ceramic foams having pre-selected cell volume distribution with stochastic coordinates and orientations was created via a finite element analysis (FEA) software package: ANSYS^{TM}. The modeling process considers the imperfections and randomness of real foam structures with a LAMMPS program calculating cell sizes and coordinates under the spherical hypothesis of cell geometry. Second, different groups of finite element models were generated using the developed foam modeling procedure. Each of these foam specimens contains different numbers of LV-cells. To confirm the appropriate cells to be included in each foam specimen and the suitable number of specimens to be used in statistical analysis we analyzed size sensitivity. Then finite element analysis was used to calculate the effective foam Young's modulus, shear modulus, and Poisson ratio. Finally, the results obtained in this work were compared with some results in the literature. It is concluded that the approach developed in the current work yields more accurate mechanical models for open cell ceramic foams than that of other models in the literature. A few conclusions on the developed models and results are summarized in the final part.

2. Modeling

Due to the randomness and imperfection of foam manufacturing processes, the coefficient pore volume of variation ($CV(V)$) of real foams usually is in the range of 1.09 to 2.13. The volume distribution of pore volume in real foams is typically modeled as log-normal [38,39]. Therefore, the generation of randomly packed spheres with a defined log-normal distribution of volume in the computations was performed using the pre-selected coefficient of variation, $CV(V)$, and the average pore volume, $E(V)$. Foam models were created using the Laguerre-Voronoi tessellation method applied to the randomly packed spheres. We used a modeling procedure that includes four steps [40,41]:

(1) Generation of spheres with a pre-selected volume distribution (it is a log-normal distribution with variation coefficient $CV(V)$ and average value $E(V)$).
(2) Random packing of the spheres generated by (1).
(3) Applying the Laguerre-Voronoi tessellation to the randomly packed spheres from (2).
(4) Struts generation along the cell edges of Laguerre-Voronoi diagram from (3).

Figure 1 schematically shows this modeling procedure.

Steps (1) and (2) were computed in an open source software package, LAMMPS, which is normally used for molecular dynamics simulations. LAMMPS runs by reading in scripts and executing the commands. The basic idea of step (2) is to randomly "pour" spheres into the top of the simulation cell and then let them fall to the bottom under gravitational forces. A quadratic potential is applied for the pairwise interactions between any two different spheres, so they're technically real solid balls. This allows one to use a straightforward molecular dynamics simulation with gravity turned on to do the packing. A visualization software, OVITO was used to visualize steps (1) and (2). After packing spheres, the Laguerre-Voronoi tessellations were performed to generate a so-called Laguerre-Voronoi

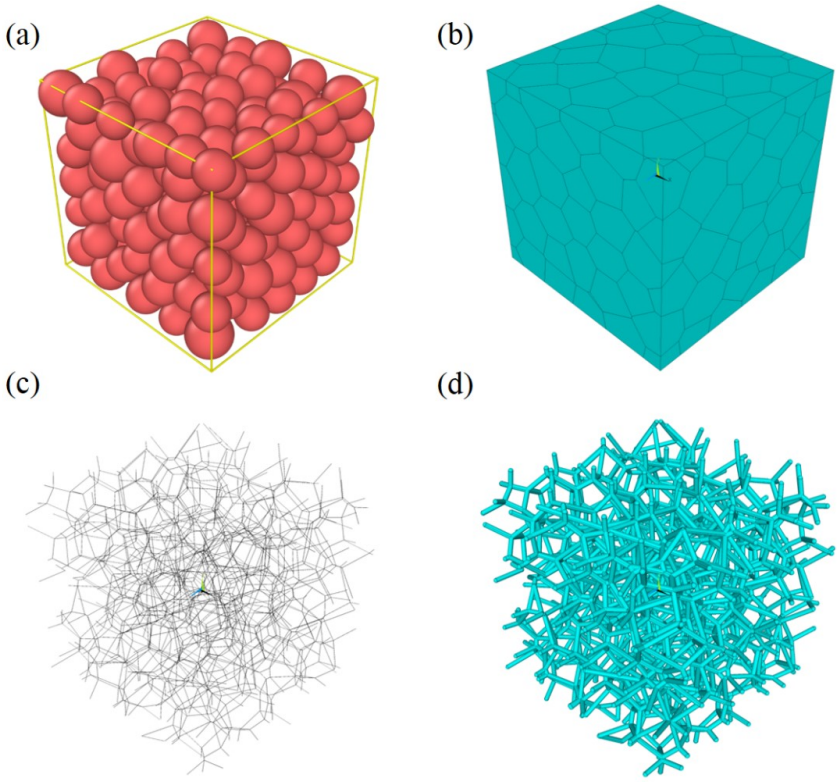

Fig. 1. Schematic illustration of the modeling procedure for generating foam structures: (a) randomly packed spheres with the pre-selected volume distribution, (b) Laguerre-Voronoi diagram based on the spheres of (a), also called LV-cells, (c) cell edges and vertices of the Laguerre-Voronoi diagram, and (d) generation of struts along the cell edges of (c)

diagram, which is a structure consisting of polyhedrons. In step (4) the struts have a constant diameter. In addition, the faces and volumes of the Laguerre-Voronoi diagram were deleted in this step. Small spheres were replaced with vertices if their diameters were less than or equal to that of the struts to make dimensions conform in the foam structures. Steps (3) and (4) were realized using a script written in the APDL language for the package ANSYS^{TM}.

TABLE 1

Structure parameters for models generated using Laguerre-Voronoi tessellation procedure

Structure (ppi)	Mean pore diameter (mm)	$CV(d)$	Mean strut diameter (mm)	Porosity (%)	Specific surface area ($\times 10^3$ m^2/m^3)
10	3.53	0.25	1.2	72.7	909.6
			1.1	75.9	893.1
			1.0	78.4	871.7
			0.8	84.0	810.4
			0.6	89.4	714.9
			0.4	94.7	568.7
20	2.44	0.265	0.8	67.0	1306.5
			0.6	76.9	1207.1
			0.55	79.5	1169.9
			0.5	82.1	1126.3
			0.4	86.6	1015.7
			0.3	92.3	791.0
30	2.08	0.28	0.8	60.0	1574.7
			0.6	71.6	1486.7
			0.55	74.2	1449.8
			0.5	77.7	1404.9
			0.4	83.6	1285.5
			0.3	89.4	1113.4

According to the structural parameters of real ceramic foams, a set of eighteen types of structures (see Table 1) were generated. The coefficient of variation for pore diameters, $CV(d)$, was from 0.25 to 0.28. For each type of structures, totally two identical structures were developed to obtain the mean value of each parameter. Variation coefficient of sphere volumes $CV(V)$ can be determined by the selected spheres in the first step of the modeling procedure. Each structure is bounded by a cubic box and includes at least 125 spheres. This number is needed to ensure that sufficient cells exist in one foam sample to study the properties of the foams, which will be discussed in the results. Strut diameters vary from 0.3 to 1.2 mm, which provides porosity ranging from 60.0% to 94.7%. Strut diameter of 1.2 mm was used to create representative structures for 10 ppi commercial ceramic foams. Figure 2 shows the foam structures generated to model commercial 10 ppi ceramic foams with different porosities: (c) 75% and (d) 95%.

3. Finite element analysis

To obtain the elastic properties of the open cell foams, a finite element study was performed using the commercial finite element analysis software ANSYS 16.0 (Ansys, Inc.,

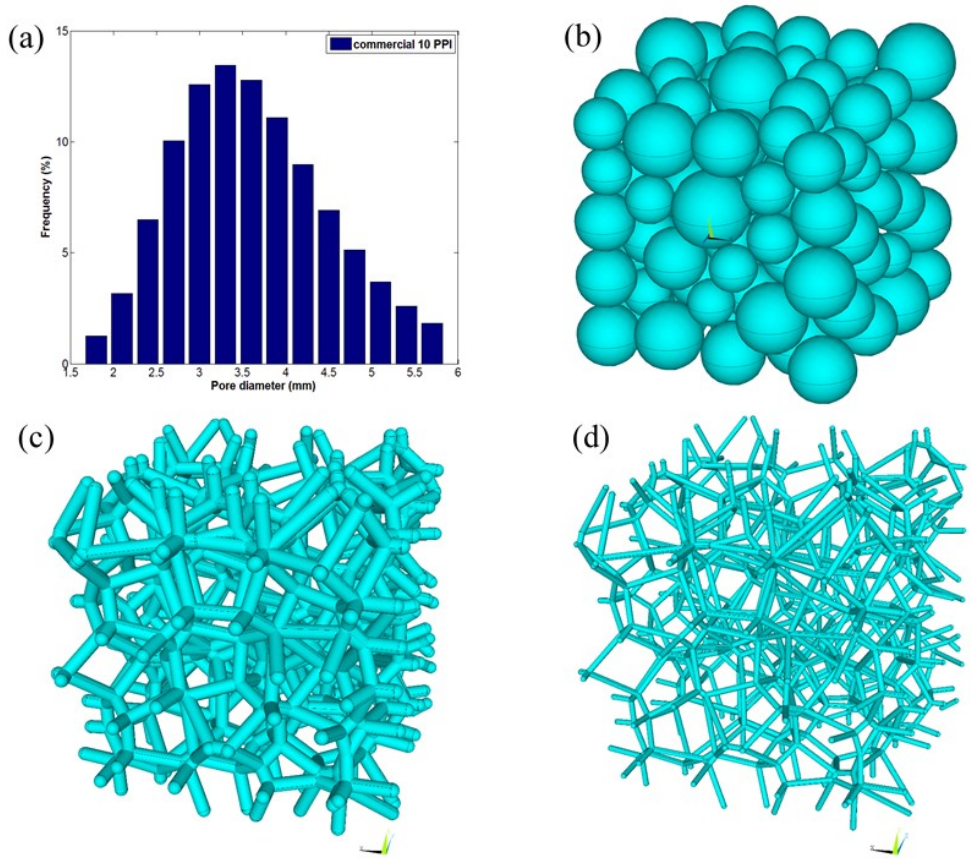

Fig. 2. Foam structures generated for commercial 10 ppi ceramic foams: (a) the pore size distribution obtained by X-ray tomography, (b) randomly packed spheres, (c) foam structure with porosity 75%, and (d) foam structure with porosity 95%

Canonsburg, PA, USA). Ceramic foams made of alumina were investigated in this work. The Young's modulus E_s and Poisson's ratio v_s of the alumina were, respectively, taken to be 370 GPa and 0.22 [42]. Each strut of the foams was modeled by Timoshenko beam elements (i.e., element type Beam189 in ANSYS which is a three-node beam element). The Timoshenko beam element works for both stout and slender beams, which involves twisting, shearing, stretching, and bending deformations. Previous studies proved that the convergence is sufficient using such a beam element to present struts [23,30-32]. Note that some short struts inevitably exist in highly irregular foam structures. Under these situations, typical beam elements are technically inappropriate for modeling short struts. However, according to the literature [43], the error resulted from using inappropriate elements could be ignored since short struts only account for a small fraction (a few percent) of the total number of struts.

In this current work, to evaluate the Poisson's ratios and effective Young's moduli of the foam with respect to the three orthogonal directions, uni-axial compressive tests on foam structures along directions, x_1, x_2 and x_3, were analyzed. In the x_1x_2 plane, the performed analyses are shown in Figure 3. For example, if strains are applied on the right and/or top sides of the sample, displacement constraints may be imposed at the left side of the sample in the x_1 direction and at the bottom side of the sample in the x_2 direction, as shown in Figure 3. The cases in x_2x_3 and x_3x_2 planes are the same as that of x_1x_2 plane. Figure 4 shows the analysis settings of ceramic foam models in ANSYS. In each case, a linear compressive strain, e.g., $\delta = -0.001$, was applied in the loading direction to avoid local buckling of struts. The Poisson's ratios, v_{12} and v_{13} and effective Young's modulus, E_1, of the foam in the x_1 direction are given by

$$E_1 = \frac{-F_1}{\delta_1 L_2 L_3} \tag{1}$$

$$v_{12} = -\frac{u_2^1}{\delta_1 L_2}, v_{12} = -\frac{u_3^1}{\delta_1 L_3} \tag{2a,b}$$

where δ_1 is the applied linear strain, and F_1 is the total reaction along x_1 direction on the defined boundary. Notation u_j^i, $i, j \in \{1,2,3\}$, stands for the lateral displacement that is in the x_j direction and is perpendicular to the loading direction x_i. The effective Young's moduli and Poisson's ratios along the x_2 and x_1 directions, E_2, E_3, v_{21}, v_{23}, v_{31} and v_{32}, can be similarly determined as:

$$E_2 = \frac{-F_2}{\delta_2 L_1 L_3} \tag{3}$$

$$v_{21} = -\frac{u_1^2}{\delta_2 L_1}, v_{23} = -\frac{u_3^2}{\delta_2 L_3} \tag{4a,b}$$

$$E_3 = \frac{-F_3}{\delta_2 L_1 L_2} \tag{5}$$

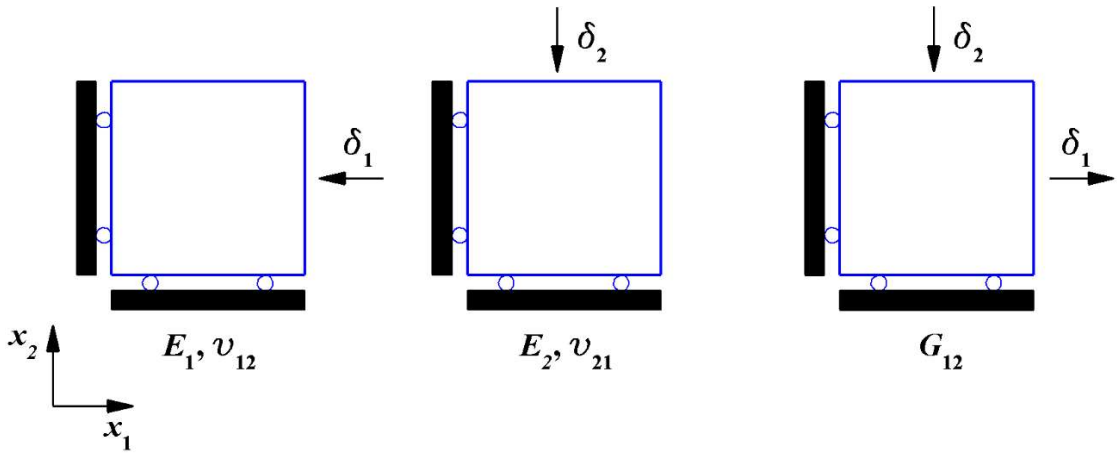

Fig. 3. Performed analyses for determining the elastic properties

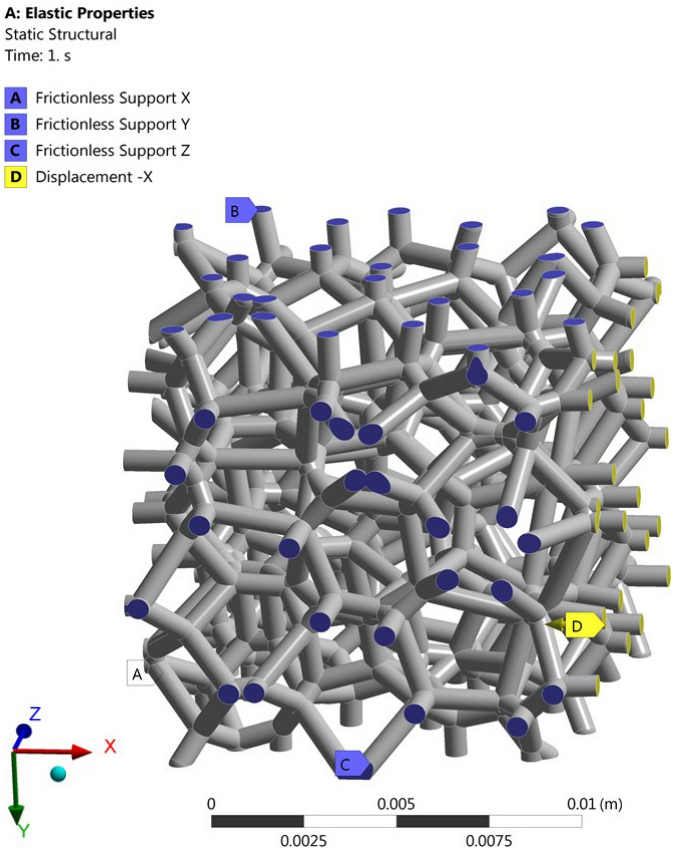

Fig. 4. Boundary conditions of ceramic foam models in ANSYS

$$\nu_{31} = -\frac{u_1^3}{\delta_3 L_1}, \nu_{32} = -\frac{u_2^3}{\delta_3 L_2} \tag{6a,b}$$

A bi-axial load testing was performed to calculate the effective shear modulus G_{12}. A small compressive strain, e.g., $\delta_1 = -0.001$, along the x_2 direction and a small tensile strain, e.g., $\delta_1 = 0.001$, along the x_1 direction was applied simultaneously (see Fig. 3). Then, the effective shear modulus G_{12}, determined by $G_{12} = \tau_{12}/\gamma_{12}$, is given by

$$G_{12} = \frac{F_1 / L_2 - F_2 / L_1}{2L_3\left(\delta_1 - \delta_2\right)} \tag{7}$$

where F_1 and F_2 are the total reaction along x_1 and x_2 directions, respectively, on the boundary. The other two shear moduli, G_{23} and G_{31}, can be similarly determined by

$$G_{23} = \frac{F_2 / L_3 - F_3 / L_2}{2L_1\left(\delta_2 - \delta_3\right)} \tag{8}$$

$$G_{31} = \frac{F_3 / L_1 - F_1 / L_3}{2L_2\left(\delta_3 - \delta_1\right)} \tag{9}$$

In addition to displacement boundary conditions, the condition of the spatial periodic boundary was applied to avoid underestimating foams' elastic properties [31,32]. The samples obtained by the procedure described in this current work can be viewed as periodic since the samples are representative of an infinite foam structure. That is, each node on one side (e.g., h^+) has a paired node on the opposite side of the sample (e.g., h^-), as shown in Figure 5. For uni-axially deformed samples under the prescribed strain δ_i, the periodic boundary conditions can be expressed by

$$u_i^{k^+} - u_i^{k^-} = \delta_i\left(x_i^{k^+} - x_i^{k^-}\right), \omega_i^{k^+} - \omega_i^{k^-} = 0, i \in \{1,2,3\} \tag{10a,b}$$

where $x_i^{k^+}$ and $x_i^{k^-}$ are the positions of the paired nodes k^+ and k^- on the boundary faces of the samples, respectively; $u_i^{k^+}$ and $u_i^{k^-}$ are the normal displacements of k^+ and k^-, respectively; $\omega_i^{k^+}$ and $\omega_i^{k^-}$ are the rotations of paired notes k^+ and k^-, respectively. In addition, Equation (10) is valid only for foams undergoing small deformations. Non-periodic localized deformations might occur when foams are subjected to a large strain and periodic boundary conditions therefore cannot be applied [16,17].

The periodic boundary conditions described in Equation (10) can be performed by defining four reference nodes N0, N1, N2, and N3. These four reference nodes introduce three two-node axial elements E01, E02, and E03, as shown in Figure 5. Four reference nodes can only move along their axial elements. Equation (10) can be rewritten as

$$u_i^{k^+} - u_i^{k^-} - \frac{x_i^{k^+} - x_i^{k^-}}{X_i^{K^+} - X_i^{K^-}}\left(U_i^{K^+} - U_i^{K^-}\right) = 0 \tag{11a}$$

$$\omega_i^{k^+} - \omega_i^{k^-} - \left(\Omega_i^{K^+} - \Omega_i^{K^-}\right) = 0, i \in \{1,2,3\} \qquad (11b)$$

in which U_i, Ω_i and X_i are the displacements, rotations and positions of the reference nodes, respectively; the superscript K^+ stands for reference nodes Ni, $i \in \{1,2,3\}$ and the superscript K^- denotes the reference node N0. For uni-axial compressive loading in direction $-e_3$, for example, N0 is fixed and a displacement corresponding to $\delta = -0.001$ is imposed at N3.

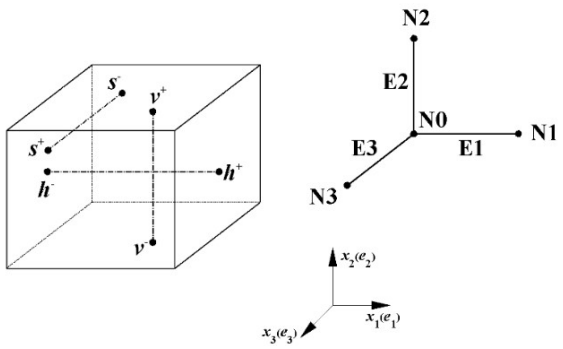

Fig. 5. Paired nodes for applying periodic boundary conditions in spatial

Due to the complicated geometries, tetrahedron elements are used for meshing foam structures generated in this current work. A large number of elements with large degrees of freedom are in the finite element models after meshing. For instance, the 125-cells model with 90% porosity consists of approximately 1,200,000 quadratic 10-node tetrahedron elements, approximately 2,000,000 nodes, and approximately ten million degrees of freedom. The number of elements and degrees of freedom would increase if the porosity of the model decreases. Additionally, one typically increases the number of elements to perform convergence tests in the analyses. Examples of meshes generated on foam structures are shown in Figure 6.

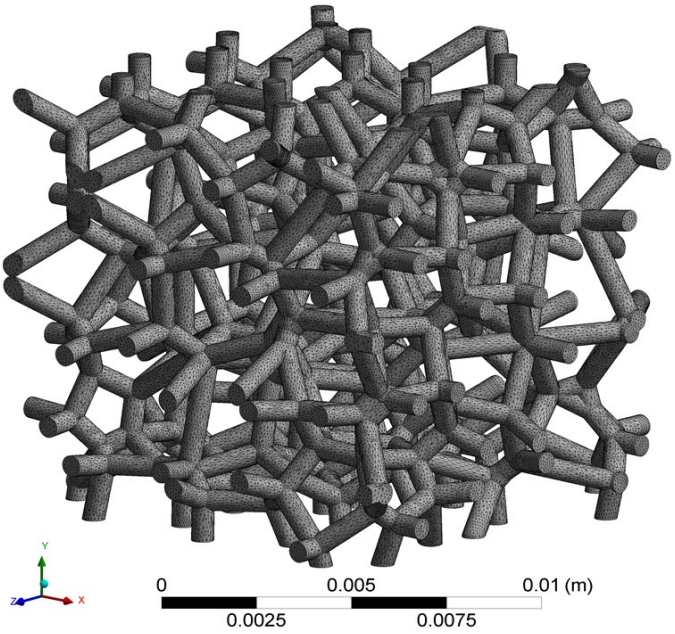

Fig. 6. Examples of meshed foam models for finite element analysis

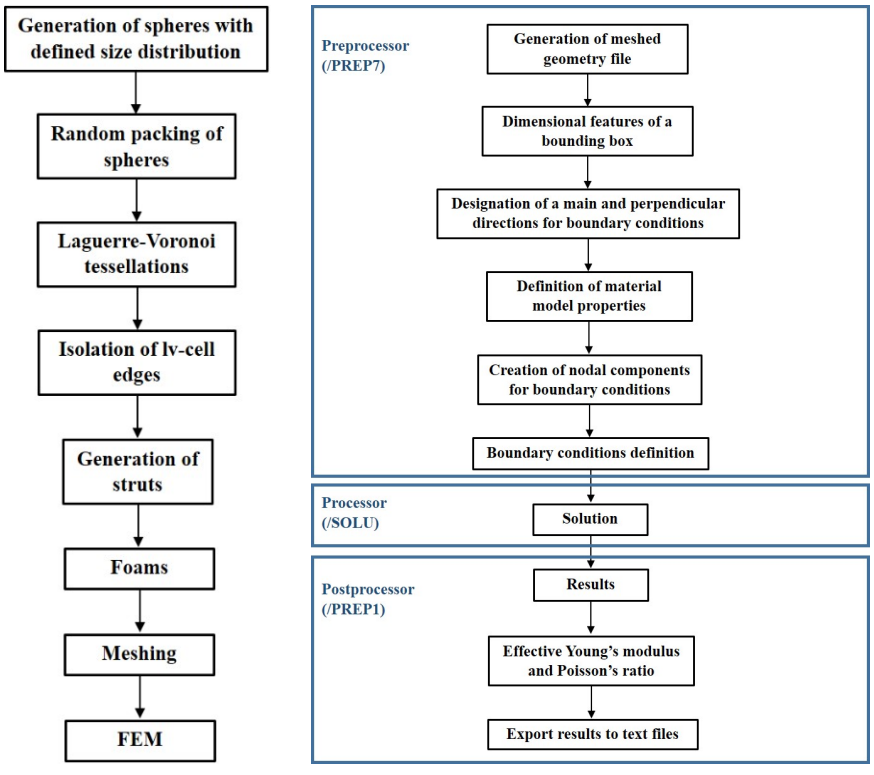

(a) (b)

Fig. 7. (a) Schematic illustration of procedures for modeling foam structures, and (b) FEA algorithm for evaluating elastic properties of foam structures

In conclusion, to investigate the elastic properties of open cell foams, an FEA algorithm was developed using the APDL language. The method includes generating a meshed geometry file, applying boundary conditions, defining solution parameters, computing results, post-processing obtained data and writing them into user files. Based on the procedure and equations discussed in the paper, Figure 7 shows the developed procedure for the investigation of foam structures' elastic properties using meshed geometry and FEA.

4. Results and discussion

4.1. Sensitivity of model size

Before proceeding to model three-dimensional foams, one should consider how many cells should be involved in one sample. Since the foam models generated in this current work have randomness and imperfections, analyses on a foam sample having only a few cells might introduce

non-trivial errors to results, and thus definitive conclusions could not be made about the macroscopic properties. On the other hand, too many cells in one foam sample would require more computing resources and be very time-consuming. Therefore, choosing a balance between reliable results and computational costs is an important modeling consideration.

The size or volume of a representative sample or element and the number of samples play a critical role in the physics and mechanics of random heterogeneous materials to evaluate the effective properties in a finite element analysis. Kanit et al. [44] reported that for a given desired precision and number of samples, a minimal volume of representative sample for prediction of effective properties can be obtained. Their results can also estimate the minimal number of samples that must be considered for a given volume of samples with a view to calculating the effective properties for a desired precision. Therefore, the size and number of samples need to be carefully selected for precise predictions. For the current work, five different scales of foam models were considered: C-2, C-3, C-4, C-5, and C-6 corresponding to foam specimens with 2 × 2 × 2, 3 × 3 × 3, 4 × 4 × 4, 5 × 5 × 5, and 6 × 6 × 6 cells, respectively. In each model, ten random foam specimens with a porosity of approximate 90% based on five different kinds of commercial alumina ceramic foams: 10 ppi, 20 ppi, 30 ppi, 40 ppi, and 50 ppi, were generated to calculate the average and standard deviation of effective properties. The foam specimens are loaded by the uni-axial compression. The effective elastic properties, e.g., Young's modulus, Poisson's ratio, and shear modulus, can be obtained from Equations (1)-(10). The obtained numerical results of E_1, E_2, E_3, ν_{12}, ν_{23}, ν_{31}, G_{12}, G_{23}, and G_{31} are shown in Figures 8-10.

Figures 8-10 show that the mean of Poisson's ratios is roughly invariant as the number of cells varies while the effective Young's modulus and shear moduli decrease with increasing the size of specimens. The standard deviations (error bars in Figs. 8-10) of all elastic constants decrease significantly with the increase of the number of cells from 8 to 125. When the number of cells is equal to 125, the standard deviation is less than 5% of the mean for all constants. Although small fluctuations exist, further increases in the number of cells do not lead to obvious changes in the values of standard deviation. Based on this result, the specimens having 125-cells were selected as the representative samples for the further finite element analyses.

4.2. Effects of porosity (or relative density)

With the aim of obtaining the definitive mechanical responses of foam models under defined testing in this work, a set of distinct cross-sections in the direction of loading was analyzed as shown in Figure 11. Figure 12 shows the numerical results of alumina foam models under uni-axial compression loading.

Figure 13 shows the numerical results of alumina foam models underbi-axial loading. Figure 14 and Figure 15 show that the overall results of the alumina foam model under uni-axial and bi-axial loading.

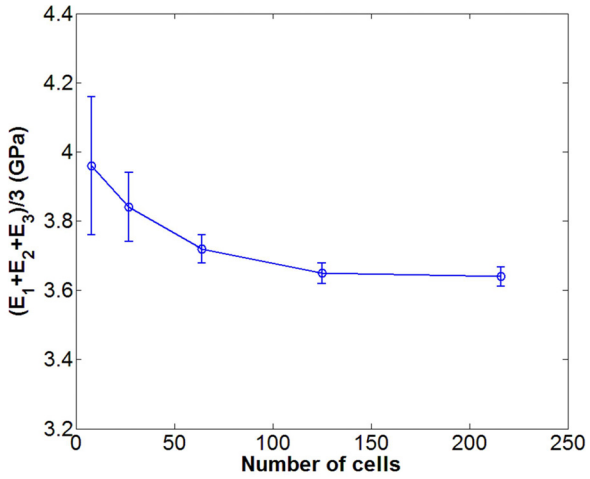

Fig. 8. Young's moduli vs. the number of cells

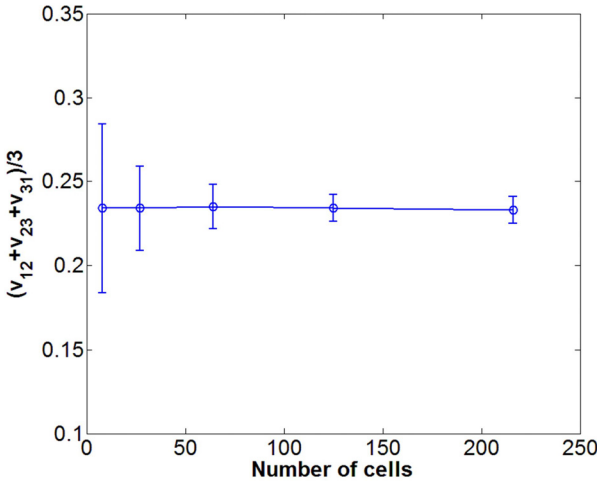

Fig. 9. Poisson's ratio vs. the number of cells

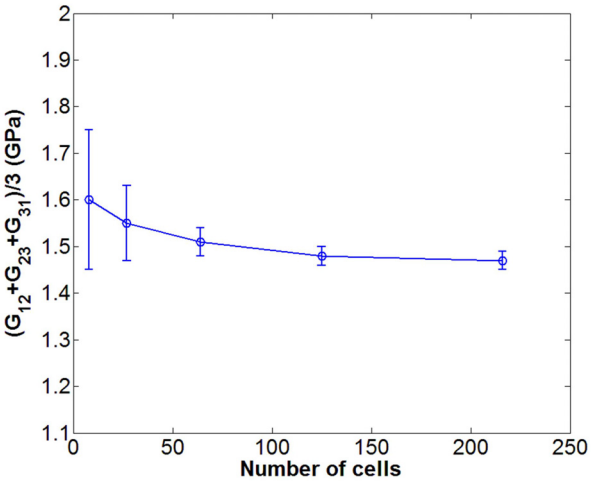

Fig. 10. Shear moduli vs. the number of cells

Some of the open cell foam models in the literature were compared with the results of finite element analyses done in this work. Gibson et al. [7] suggested that for a foam represented by cubic unit cells Young's modulus and bulk modulus of open cell foams are proportional to relative density squared and rela-

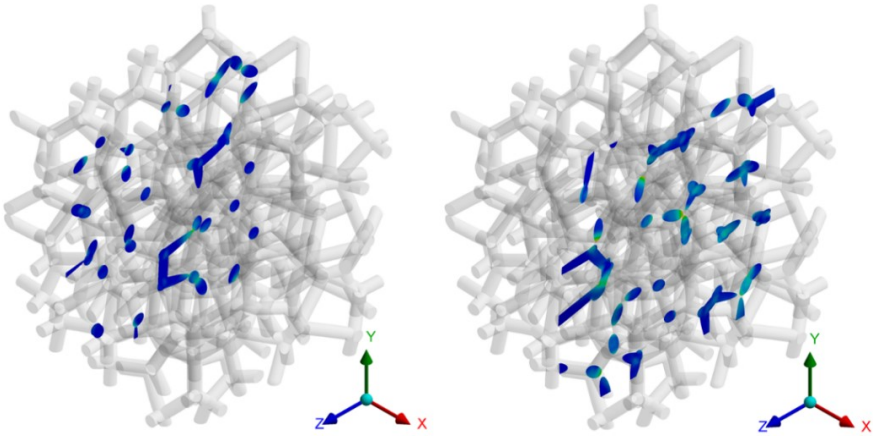

Fig. 11. Two of distinct cross-sections in the direction of loading: cross-section 4 (left) and 8 (right)

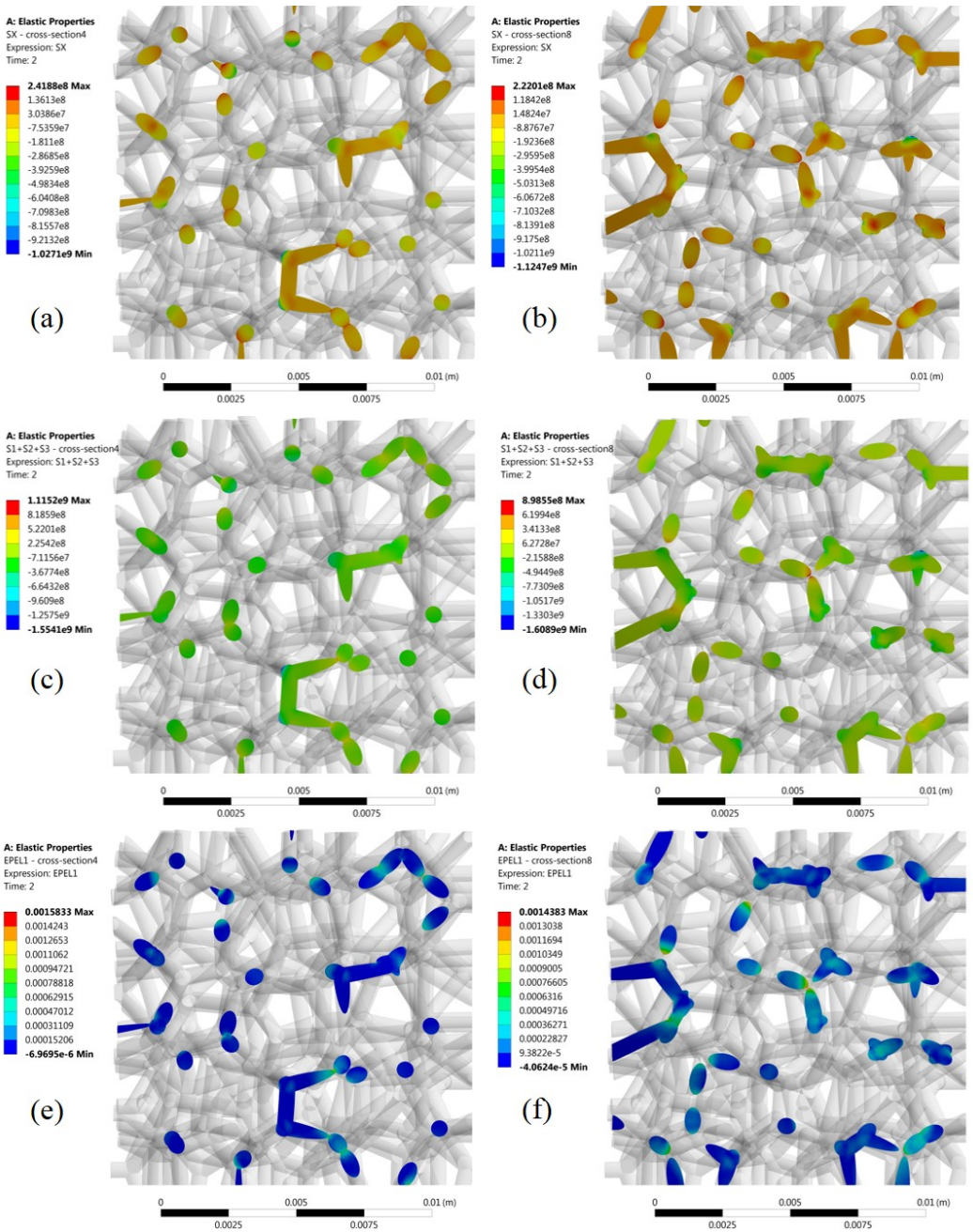

Fig. 12. Finite element analysis results: (a), (c), and (e) are, respectively, normal stress, total stress, and strain of cross-section 4; (b), (d), and (e) are, respectively, normal stress, total stress, and strain of cross-section 8 under uni-axial loading in *x* direction

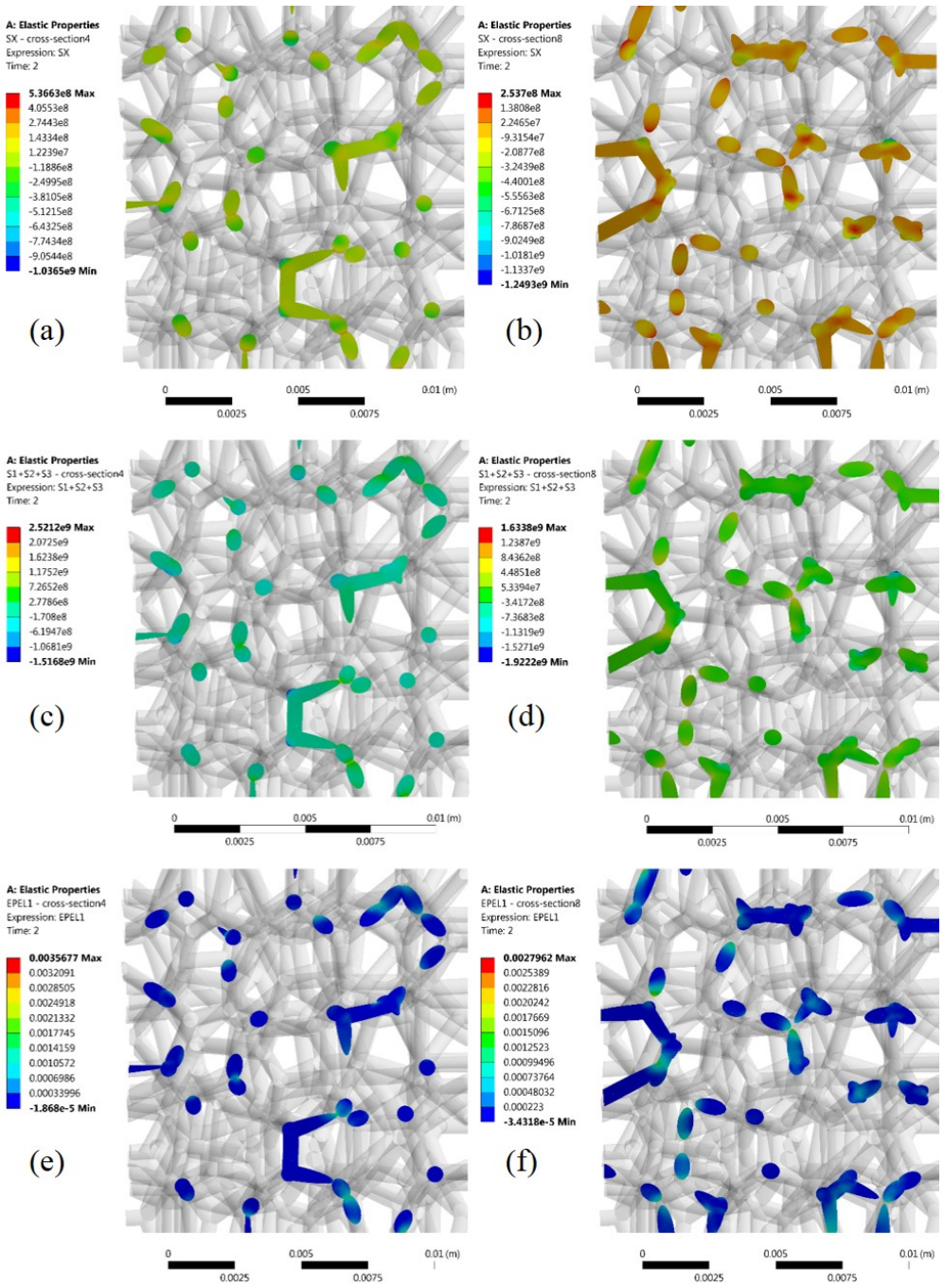

Fig. 13. Finite element analysis results: (a), (c), and (e) are, respectively normal stress, total stress, and strain of cross-section 4; (b), (d), and (e) are, respectively, normal stress, total stress, and strain of cross-section 8 under bi-axial loading in x and y directions

tive density, respectively. Their work also indicates that under hydrostatic loading and uni-axial load the bending and stretching of foam struts are the major deformation of open cell foams, respectively. This conclusion has been verified by other work with models using a Kelvin cell instead of the cubic cell [18-20,45]. Additionally, Zhu et al. [28] have found the relationship between mechanical properties of open cell foams modeled by Voronoi tessellation and the relative density. In the small relative density regime, the deformation mechanism of Voronoi foams is similar to that of Kelvin foams. The effects of the porosity (or relative density) of foam models on its elastic properties of were also considered in this work. Note that in our investigation the foam models of the same morphological structure but different porosities are obtained by varying the diameter of foam struts.

Warren et al. [9] developed a three-dimensional foam model using the tetrahedral unit cell to investigate the macroscopic properties of open cell foams. The effective Young's modulus and Poisson's ratio for uniform struts are given by [9]:

$$E = \frac{E_s \varphi^2 (11 + 4\varphi)}{(10 + 31\varphi + 4\varphi^2)} \tag{12}$$

$$\nu = \frac{(1-\varphi)(5+4\varphi)}{(10+31\varphi+4\varphi^2)} \tag{13}$$

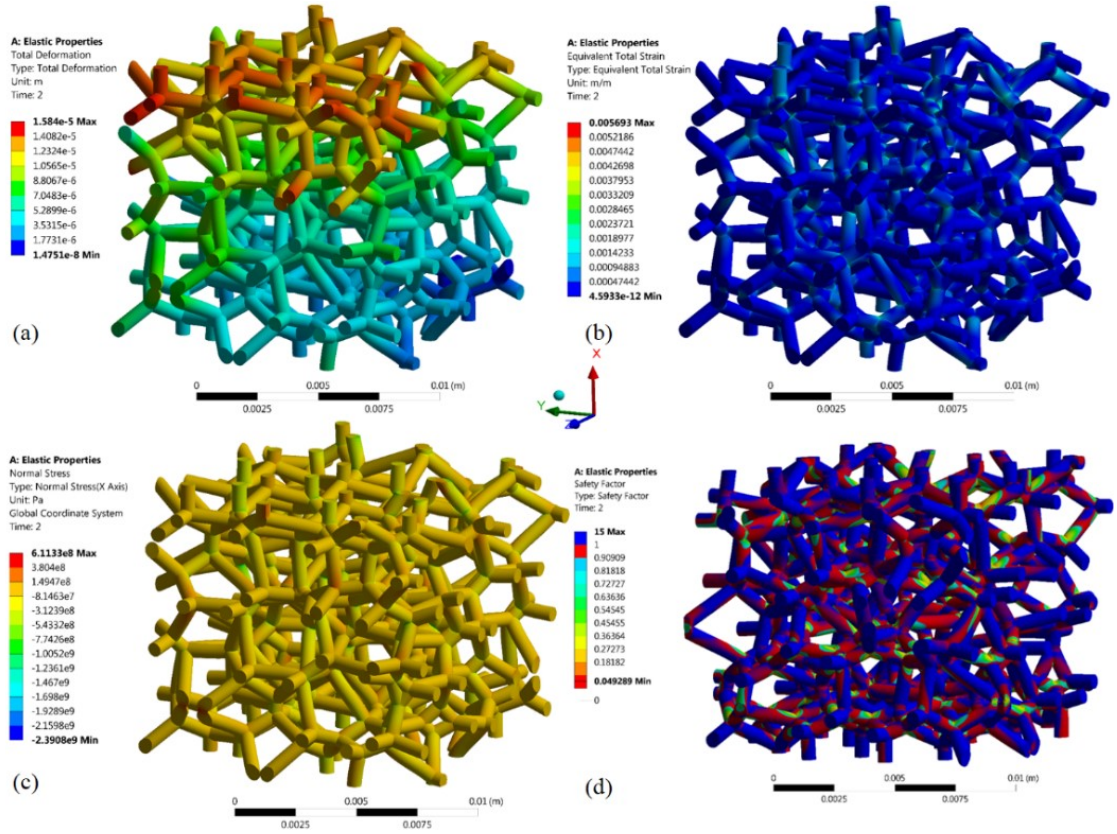

Fig. 14. Total numerical results of alumina foam models under uni-axial loading: (a) total deformation, (b) equivalent total strain, (c) normal stress, and (d) safety factor

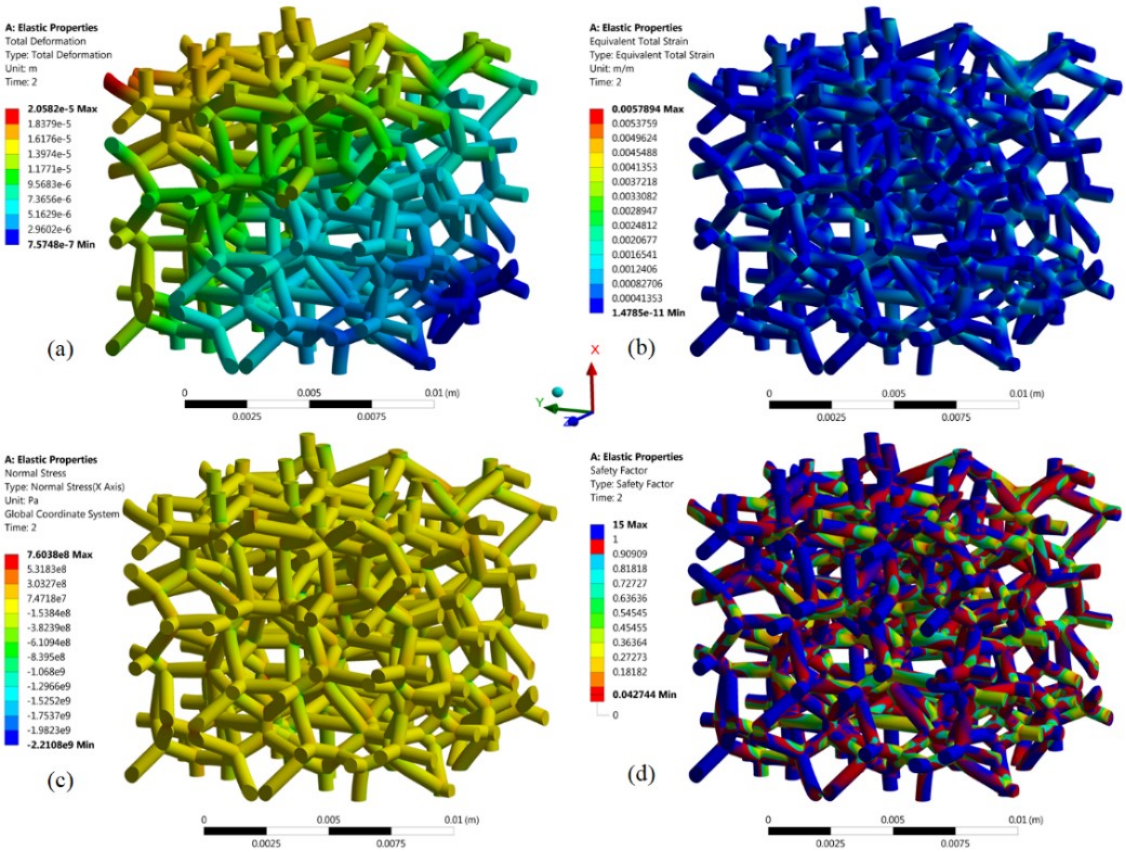

Fig. 15. Total numerical results of alumina foam models under bi-axial loading: (a) total deformation, (b) equivalent total strain, (c) normal stress, and (d) safety factor

in which E_s is the Young's modulus of the strut material (here taken as 370 GPa). The relative density φ is equal to $1-\varepsilon$. ε is porosity of foams. Relative density is defined as the ratio between the volume of solid material and total volume of the bulk geometry, which can be given as $\varphi = \rho/\rho_s$.

The model proposed by Zhu et al. yields similar equations for the mechanical properties of Kelvin foams as follows [20]:

$$E = \frac{1.009E_s\varphi^2}{1+1.514\varphi} \tag{14}$$

$$\nu = 0.5\frac{1-1.514\varphi}{1+1.514\varphi} \tag{15}$$

$$G = \frac{0.32E_s\varphi^2}{1+0.96\varphi} \tag{16}$$

Three-dimensional Voronoi models without imperfections were developed by Gan et al. [23]. In that study, three-dimensional random Voronoi cells were used to construct the open cell foams for predicting the elastic constants. The curves fitting to the results of finite element analysis yield [23]:

$$E = \frac{E_s\varphi^2}{1+6\varphi} \tag{17}$$

$$\nu = \nu_s + (0.5-\nu_s)\frac{1-\varphi}{1+14\varphi} \tag{18}$$

where ν_s is Poisson's ratio of alumina, 0.22.

Roberts et al. [26] adopted a random Voronoi tessellation technique to simulate the deformation mechanism of open cell foams under external loadings. Gibson et al. [7] derived an equation, $E = E_sC(1-\varepsilon)^n$, to fit the results reported by Roberts et al. The parameters C and n were found as 0.93 and 2.04, respectively, for the high porosity foams, i.e., $0.90 < \varepsilon < 0.96$. Since Poisson's ratio is taken as a constant through the study by Roberts et al., here this work only presents Young's modulus formula which is expressed as [26]:

$$E = 0.93E_s\varphi^{2.04} \tag{19}$$

Figures 16-18 show the Young's modulus E, Poisson's ratio ν, and shear modulus G for FEA foam models having different porosity values, and the comparison with other researchers' results.

Curve fitting the numerical results yields:

$$E = E_s\left[3.32(1-\varphi)^3 - 7.37(1-\varphi)^2 + 4.98(1-\varphi) - 0.92\right] \tag{20}$$

$$\nu = \nu_s\left[20.68(1-\varphi)^3 - 42.09(1-\varphi)^2 + 30(1-\varphi) - 6.91\right] \tag{21}$$

Equations ((12)-(21)) are included in Figures 16-18 for the purpose of comparison. Observe in Figure 16 that, in the range of high porosity ($90\% < \varepsilon < 95\%$), results (20) and (21) for alumina foam models developed in our current work are close to those of Kelvin foams (12)-(19): the disparity is normally no more than 1%. In addition, Zhu et al. [20] also pointed out slightly different results for Voronoi foams. Even at a very high value of ε (i.e., $\varepsilon >$ 96%), they found that the estimated Young's modulus of Kelvin foams is 50% less than that of Voronoi foams while the bulk modulus of Kelvin foams is approximate 20% greater than that

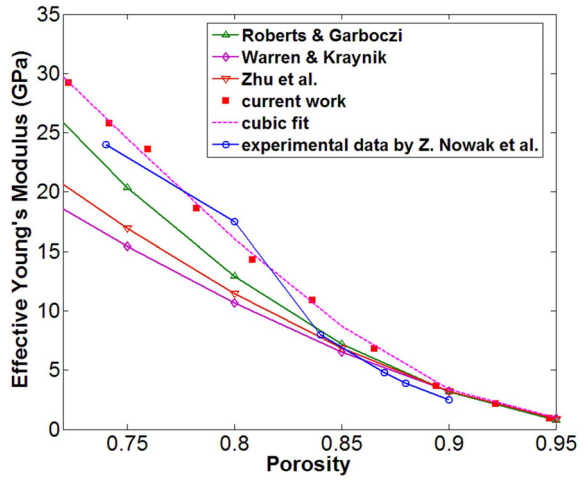

Fig. 16. Effective Young's modulus variation with porosity

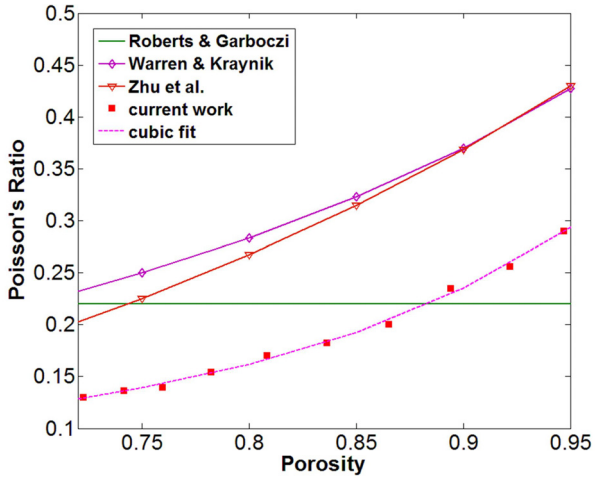

Fig. 17. Poisson's ratio variation with porosity

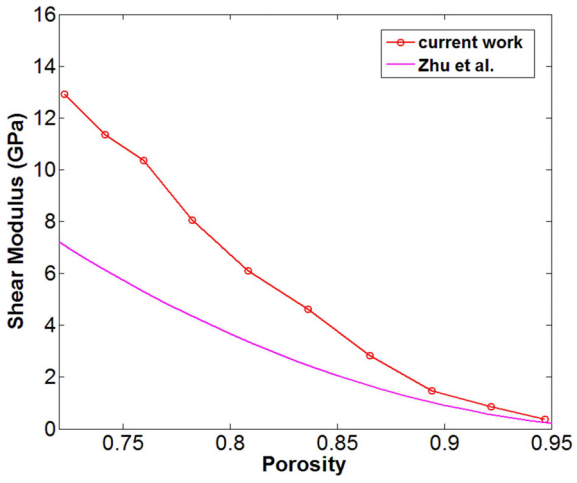

Fig. 18. Shear modulus variation with porosity

of Voronoi foams. The exact reason for the difference between the results of Voronoi foams and Kelvin foams cannot be readily identified. Also, the results of Laguerre-Voronoi foams in this work is closer to those of Voronoi foams by Robarts and Garboczi than Kelvin cells. Such a phenomenon is not hard to understand since Laguerre-Voronoi foams and Voronoi foams have similar generation algorithms and thus similar foam structure. As seen in Fig. 16 , the results of this current work generally are also in a good agreement with the experimental data by Z. Nowak et al., who studied the elastic responses of alumina foams with porosity of 74-90% under compression loadings [42]. For smaller values of ε, however, Fig. 16 shows that the Young's modulus of foam models in this work (Equation(20)) diverges significantly from perfect Kelvin foams (Equation(14)). The reason for this could be that the current numerical analysis used Timoshenko beam theory. This approach is appropriate for stout beams only, corresponding to foams with moderate or even small porosity ε, whilst the solutions (14)-(15) by Zhu et al. [20] are based on Euler-Bernoulli beam theory and thus are suitable for foams with large ε. Furthermore, for real open cell foams the struts with lower porosity (e.g., less than 80%) cannot be simply modeled as uniform beams any more. The plateau border effect would be predominant in those cases [9,11]. This might be the major reason that the results for lower porosity in the comparison studies deviate significantly from each other.

From Figure 17, note that the Poisson's ratio of this work has a similar trend as two other theoretical models: the tetrahedral cell model by Warren and Kraynik and the Kelvin cell model by Zhu et al. However, the amplitude of variation of this work is smaller than those of these two theoretical models. Moreover, the Poisson's ratio results of this work are close to the constant assumption of Roberts and Garboczi, i.e., assuming a constant Poisson's ratio is acceptable. The results of this current work verify the constant assumption of Poisson's ratio in open cell foams. As for the shear modulus, Figure 18 shows that results of the current model are in a good agreement with that of the Kelvin cell model by Zhu et al. when porosity is greater than 90%. The shear modulus predictions of these two models have a big difference at low porosity (say <85%).

5. Conclusions

The main benefit of this study is the development of three-dimensional random Laguerre-Voronoi FEA models (in ANSYS^{TM}). The proposed method can accurately generate foam models having randomly distributed parameter values. A three-dimensional model of ceramic foams having pre-selected cell size distribution with random coordinates and orientations was created using ANSYS^{TM}. Different groups of finite element models were then generated. The size sensitivity study presents that each of foam specimens at least contains 125 LV-cells.

The developed foam models were used to simulate the macroscopic elastic properties of open cell foams under uni-axial and bi-axial loading and were compared with existing open cell foam models in the literature. In the high porosity regime, it is found that the elastic properties predicted by random Laguerre-Voronoi foam models are almost the same as those by perfect Kelvin foam models while in the low porosity regime the results of the present work deviate significantly from those of other published models. However, the results of the current work generally are in a better agreement with experimental data than other models. The Laguerre-Voronoi foam models generated in this work are quite close to the topology of real foams and thus yield more accurate results than other open cell foam models considered.

Acknowledgments

The financial support of Master Dynamics of Hong Kong through Grant No. 00041200 and the National Science Foundation of China through Grant No. 51577007 is acknowledged with thanks. The authors thank Dr. Peter Hodges for proof reading the manuscript.

REFERENCE

[1] L.J. Gibson, M.F. Ashby, The mechanics of three-dimensional cellular materials. in Proceedings of the Royal Society of London A: Mathematical, Physical and Engineering Sciences. 1982. The Royal Society.

[2] L.J. Gibson, M.F. Ashby, Cellular solids: structure and properties. 1999: Cambridge university press.

[3] R.M. Stone, Strength and stiffness of cellular foamed materials. 1997, The University of Arizona.

[4] T. Nieh, K. Higashi, J. Wadsworth, Mater. Sci. Eng. A. **283** (1), 105-110 (2000).

[5] M.V. Twigg, J.T. Richardson, Chem. Eng. Res. Des. **80** (2), 183-189 (2002).

[6] M.F. Ashby, T. Evans, N.A. Fleck, J. Hutchinson, H. Wadley, L. Gibson, Metal Foams: A Design Guide. 2000: Elsevier.

[7] L.J. Gibson, M. Ashby, C. Solids, Cellular Solids, 307-308 (1997).

[8] J. Banhart, Prog. Mater Sci. **46** (6), 559-632 (2001).

[9] W. Warren, A. Kraynik, J. Appl. Mech. **55** (2), 341-346 (1988).

[10] N. Triantafyllidis, M. Schraad, J. Mech. Phys. Solids. **46** (6), 1089-1124 (1998).

[11] C. Chen, T. Lu, N. Fleck, J. Mech. Phys. Solids. **47** (11), 2235-2272 (1999).

[12] S. Papka, S. Kyriakides, Int. J. Solids Struct. **36** (29), 4397-4423 (1999).

[13] S. Papka, S. Kyriakides, Int. J. Solids Struct. **36** (29), 4367-4396 (1999).

[14] S. Gu, T. Lu, A. Evans, Int. J. Heat Mass Transfer. **44** (11), 2163-2175 (2001).

[15] W. Warren, A. Kraynik, J. Appl. Mech. **58** (2), 376-381 (1991).

[16] L. Gong, S. Kyriakides, W.-Y. Jang, Int. J. Solids Struct. **42** (5), 1355-1379 (2005).

[17] L. Gong, S. Kyriakides, Int. J. Solids Struct. **42** (5), 1381-1399 (2005).

[18] W. Warren, A. Kraynik, J. Appl. Mech. **64** (4), 787-794 (1997).
[19] W. Warren, M. Neilsen, A. Kraynik, MeReC. **24** (6), 667-672 (1997).
[20] H. Zhu, N. Mills, J. Knott, J. Mech. Phys. Solids. **45** (11), 1875-1904 (1997).
[21] T. Wejrzanowski, J. Skibinski, J. Szumbarski, K. Kurzydlowski, Comput. Mater. Sci. **67**, 216-221 (2013).
[22] J.L. Grenestedt, K. Tanaka, Scripta Mater. **40** (1), 71-77 (1998).
[23] Y.X. Gan, C. Chen, Y.P. Shen, Int. J. Solids Struct. **42** (26), 6628-6642 (2005).
[24] V. Shulmeister, M. Van der Burg, E. Van der Giessen, R. Marissen, Mech. Mater. **30** (2), 125-140 (1998).
[25] A.P. Roberts, E.J. Garboczi, Acta Mater. **49** (2), 189-197 (2001).
[26] A.P. Roberts, E.J. Garboczi, J. Mech. Phys. Solids. **50** (1), 33-55 (2002).
[27] H. Zhu, A. Windle, Acta Mater. **50** (5), 1041-1052 (2002).
[28] H. Zhu, J. Hobdell, A. Windle, Acta Mater. **48** (20), 4893-4900 (2000).
[29] J.L. Grenestedt, F. Bassinet, IJMS. **42** (7), 1327-1338 (2000).
[30] J.-q. Li, F. Luo, D.-m. Zhu, W.-c. Zhou, Transactions of Nonferrous Metals Society of China. **16**, 487-489 (2006).
[31] K. Li, X.L. Gao, G. Subhash, Int. J. Solids Struct. **42** (5-6), 1777-1795 (2005).
[32] K. Li, X.L. Gao, A.K. Roy, Composites Part B: Engineering. **36** (3), 249-262 (2005).
[33] K. Ćwieka, T. Wejrzanowski, K. Kurzydłowski, Arch. Metall. Mater. **62** (1), 259-262 (2017).
[34] B. Maruyama, J.E. Spowart, D.J. Hooper, H.M. Mullens, A.M. Druma, C. Druma, M.K. Alam, Scripta Mater. **54** (9), 1709-1713 (2006).
[35] J.R. H, H.X Zhu, A.H. Windle, Acta Mater. **48** (20), 4893-4900 (2000).
[36] J. Zhou, J. Skibinski, K. Cwieka, T. Wejrzanowski, K.J. Kurzydlowski, O. Adiguzel, MATEC Web of Conferences **30**, 03005 (2015).
[37] J. Zhou, T. Wejrzanowski, J. Skibinski, K. Cwieka, K.J. Kurzydlowski, O. Adiguzel, MATEC Web of Conferences **30**, 03006 (2015).
[38] K. Okazaki, H. Conrad, Transactions of the Japan Institute of Metals. **13** (3), 198-204 (1972).
[39] F. Rhines, B. Patterson, Metall. Trans. A. **13** (6), 985-993 (1982).
[40] Z. Nie, Y. Lin, Q. Tong, Comput. Mater. Sci. **131**, 160-169 (2017).
[41] Z. Nie, Y. Lin, Q. Tong, Int. J. Heat Mass Transfer. **113**, 819-839 (2017).
[42] Z. Nowak, M. Nowak, R.B. Pęcherski, M. Potoczek, R.E. Śliwa, Arch. Metall. Mater. **60** (3), 1957-1963 (2015).
[43] M. Van der Burg, V. Shulmeister, E. Van der Geissen, R. Marissen, Journal of Cellular Plastics **33** (1), 31-54 (1997).
[44] T. Kanit, S. Forest, I. Galliet, V. Mounoury, D. Jeulin, Int. J. Solids Struct. **40** (13), 3647-3679 (2003).
[45] H.X. Zhu, J.F. Knott, N.J. Mills, J. Mech. Phys. Solids. **45** (3), 319-343 (1997).